J Mol Model (2011) 17:1381–1392
DOI 10.1007/s00894-010-0833-2

ORIGINAL PAPER

Theoretical studies and vibrational spectra of *1H*-indole-3-acetic acid. Exploratory conformational analysis of dimeric species

Rosana Maria Lobayan · María Celia Pérez Schmit · Alicia H. Jubert · Arturo Vitale

Received: 12 July 2010 / Accepted: 22 August 2010 / Published online: 14 September 2010

Abstract Theoretical studies on *1H*-indole-3-acetic acid (IAA) were performed to investigate the conformational properties of dimeric species and vibrational spectra. Experimental infrared spectra at 100 K and 297 K and Raman spectrum at 297 K were analyzed and compared against calculations performed at B3LYP/6-31G** level. A exploratory study of the conformational space of dimeric species was performed. Our analysis showed that dimeric forms predicted theoretically contribute distinctively to the assignments of experimental results. These structures are defined by the orientation of the acetyl moieties with respect to the plane of indole ring. The dimers are formed by two symmetrical IAA monomers (one of them with the acetyl moiety upward oriented, *Re*-face, and the other isomer having the acetyl moiety downward oriented, *Si*-face) in tail-to-tail way. The X-ray geometry and FTIR vibrational frequencies were compared with the results of DFT calculations. A conformational equilibrium involving the non-equivalent IAA dimers: CCT-CCT, $A^{+}A^{+}T$-$A^{-}A^{-}T$, $A^{+}A^{-}T$-$A^{-}A^{+}T$, and $A^{+}CT$-$A^{-}CT$ was found. The relation of the conformational properties of the IAA molecule with the features of the vibrational spectra was described in detail. The band assignments were discussed as related to the conformations properties. Our analysis shows the significance of the theoretical study of the conformational space of the monomeric molecule in the rationalization of experimental results.

Keywords Density functional theory · 1H-Indole-3-Acetic Acid (IAA) · Infrared spectroscopy · Raman spectroscopy

Rosana Maria Lobayan and María Celia Pérez Schmit contributed equally to this work

Electronic supplementary material The online version of this article (doi:10.1007/s00894-010-0833-2) contains supplementary material, which is available to authorized users.

R. M. Lobayan (✉) · M. C. Pérez Schmit
Facultad de Ingeniería, Universidad de la Cuenca del Plata,
Lavalle 50,
3400 Corrientes, Argentina
e-mail: rlobayan@ucp.edu.ar

A. H. Jubert
CEQUINOR Facultad de Ciencias Exactas y Facultad de Ingeniería, Universidad Nacional de La Plata,
CC 962,
1900 La Plata, Argentina

A. Vitale
PRALIB (UBA, CONICET), Facultad de Farmacia y Bioquímica,
Universidad de Buenos Aires,
Junín 956,
C1113AAD Buenos Aires, Argentina

Introduction

The indole ring of the IAA (Fig. 1) occurs in many compounds that exhibit very important biological activity, e.g., hormonal activity (plant growth regulator: auxin compounds), and serotonergic activity (tryptamine, serotonine, etc). A heteroaromatic indole ring, and a carboxylic side chain are the two systems that combine to form IAA. As the monofunctional carboxylic acids regularly form cyclic dimers with a eight-membered planar ring with two intermolecular O–H···O hydrogen bonds, we can expect the same intermolecular H-bonds between IAA monomers thus constituting IAA dimers. Several references report on the identification and quantitation of IAA. Usually, the theoretical study has been addressed to show the behavior and properties of substituted IAA. Many studies have been carried out by different experimental and theoretical methodology, among them, a chemometric and molecular

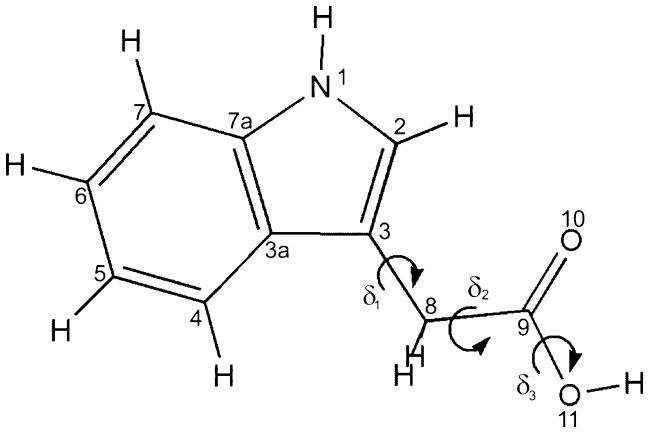

Fig. 1 Heteroaromatic planar indole ring and an acetyl side chain of IAA backbone. Dihedral angles (δ_1: $C_2—C_3—C_8—C_9$, δ_2: $C_3—C_8—C_9—O_{10}$, δ_3: $C_8—C_9—O_{11}—H$) defines distinct orientations of acetyl side chain with respect to the ring

modeling study of IAA derivatives with auxin activity has been reported [1, 2]. Another similar study related to IAA was reported by the same authors [3]. In the mentioned papers only the crystal structure was taken into account in the optimization process for monomeric and dimeric molecules.

Other authors [4] encountered a twinned crystal for IAA. This case of twinning is characterized by the fact that one diagonal of the face is of the same length as one of the axes bordering the face. Consequently, the diagonal face can be an axis of the twin unit cell, whereas the other axis is reversed. Although other authors have also determined the structure of IAA [5–8], none of them described any twinning at all.

The IR spectrum was studied in similar compounds, such as indole-2-carboxylic (ICA) and 5-methoxyindole-2-carboxylic acids (5-MeOICA). The structure analysis of ICA revealed that two chains of ICA molecules form a planar ribbon, held together by intermolecular O–H···O and N–H···O hydrogen bonds. Both the O–H and N–H groups act as donors, while the O atom of the carboxylic group is the acceptor of two hydrogen bonds [9]. The structure analysis of 5-MeOICA showed molecular ribbons constituted by two independent molecular chains held together also by intermolecular O–H···O and N–H···O hydrogen bond interactions. The carboxylic O atom is also the acceptor of two hydrogen bonds [10]. In both cases molecular structures have been resolved using single crystal X-ray diffraction, infrared spectroscopy, and theoretical methods. The assignment was performed only for strong bands.

To our knowledge, a detailed assignment of vibrational modes of the experimental infrared and Raman spectra of IAA is lacking in literature. The aim of this work is to analyze the conformational and vibrational properties of the dimeric forms of IAA. The infrared and Raman spectroscopy at 297 and 100 K, and 297 K, respectively, are carried on. The possible dimeric conformations coexisting in the sample were characterized using the conformational space of monomeric molecules scanned previously by us [11]. The vibrational spectra of the minimum energy conformers in the dimeric forms were calculated using the density functional theory (DFT) and the assignments of the vibrational modes actives in the infrared and Raman spectra are performed. The effects of conformational changes are addressed. Moreover the IR-Raman spectra of IAA monomers are also calculated to analyze the effects of dimerization.

Experimental

The IAA was provided by Aldrich Chemical Company and purified by recrystallization from methanol / water and dried on phosphorus pentoxide. The purity was determined by CGL.

Infrared absorption spectra at 297 and 100 K of 1 cm diameter pellets, made of the IAA microcrystals, diluted in spectroscopic grade KBr, were recorded with a Perkin-Elmer GX1 FTIR interferometer in the spectral range of 400 to −4000 cm^{-1} with a resolution of 4 cm^{-1}. The samples were mounted on the cold finger of an Oxford DN 1754 cryostat.

Raman spectrum, using the 1064 nm laser line of a Nd: YAG laser as exciting source, were obtained from pure powders at 297 K in a backscattering configuration of the Bruker 66 FTIR Raman accessory.

Computational details

The conformational space for IAA monomers in vacuum was studied previously by us [11] using the MD module of the HyperChem package [12]. The geometries obtained from simulation were then optimized to an energy gradient less than 0.004 kJ mol^{-1} $Å^{-1}$ at a semiempirical level (AM1). The lowest-energy conformers of the monomeric molecules were further studied using the density functional theory as implemented in the Gaussian 03 package [13]. Geometry optimizations were performed using the Becke's three parameter hybrid functional [14] with the Lee–Yang–Parr correlation functional [15], a combination that gives rise to the well-known B3LYP method. For all the atoms the 6-31G** basis set was used.

Taking into account the disposition of the conformers in the dimer present in the crystal (Cambridge Structure Database or CSD code: INACET03) several initial structures of dimers were considered. They were constructed combining the lowest energy monomers found by MD procedure.

The vibrational spectra of the minimum energy conformers both in the monomeric and dimeric forms were then calculated using the density functional theory (DFT) at the B3LYP/6-31G** level of theory.

Results and discussion

Geometrical and conformational analysis of IAA

The backbone of IAA consists of a heteroaromatic planar indole ring and an acetyl side chain (at position 3) that can adopt several distinct orientations with respect to the ring defined by three dihedral angles (δ_1: C_2—C_3—C_8—C_9, δ_2: C_3—C_8—C_9—O_{10}, δ_3: C_8—C_9—O_{11}—H) (Fig. 1). Variations on dihedral angles give rise to several different conformers. Through the study of the conformational space in vacuum we found 14 lowest energy conformers with symmetry C_1, which in stability order are: a) CCT, b) A^+A^+T/A^-A^-T, c) A^+A^-T/A^-A^+T, d) A^+CT/A^-CT, e) G^+A^+T / G^-A^-T, A^+TC/A^-TC, f) CCC, and g) A^+CC/A^-CC [11]. They were named according to IUPAC recommendations [16], and were confirmed by absence of imaginary frequencies in the vibrational analysis.

Six pairs of them account for structures of the same energy, but differing in the orientation of the acetyl group with respect to the plane of the indole ring: one of them with the acetyl moiety upward oriented, *Re*-face, and the other isomer having the acetyl moiety downward oriented, *Si*-face. Each pair shows torsion angles δ_1, δ_2 and δ_3 of contrary sign [11].

The single crystal X-ray diffraction study indicates the occurrence of A^+CT and A^-CT conformers in the crystal. Selected experimental bond lengths and angles are listed in Table 1, along with the corresponding differences from theoretical values calculated at B3LYP/6-31G** level. The agreement between the theoretical and experimental results is quite good. Some deviations from the experimental values can be attributed to intermolecular hydrogen bonds, and other packing interactions not considered in vacuum calculations. A general shortening of the bond lengths in the crystal structure was found. As is expected for the C—H lengths the higher deviation between the calculated and experimental bond lengths was noted, because their bond lengths are crystallographically underestimated due to vibrations in crystal and X-ray diffraction (location of the electron density centroids instead of atomic centers) [17]. According to Table 1, the experimental C_9—O_{11} bond length (1.311 Å) was shorter than theoretical value by 0.048 Å, and the C_9—O_{11}—H angle increased by about 12.9°. These findings can be attributed to the resonance and the intermolecular hydrogen bonding interactions in the crystal.

Table 1 Bond lengths [Å] and bond angles [°] determined for IAA by X-ray diffraction and the differences from the corresponding theoretical parameters calculated for A^+CT monomer and A^+CT-A^-CT dimer at B3LYP/6-31G** level

	Exp.	Δ_{A^+CT}	$\Delta_{A^+CT–A^-CT}$
N_1—C_2	1.362	-0.020	-0.020
C_2—C_3	1.364	-0.008	-0.007
C_3—C_{3a}	1.428	-0.015	-0.014
C_{3a}—C_{7a}	1.394	-0.028	-0.028
C_{7a}—N_1	1.384	0.004	0.004
C_{3a}—C_4	1.403	-0.003	-0.002
C_4—C_5	1.377	-0.012	-0.012
C_5—C_6	1.387	-0.023	-0.023
C_6—C_7	1.374	-0.016	-0.016
C_7—C_{7a}	1.386	-0.013	-0.013
C_3—C_8	1.480	-0.017	-0.015
C_8—C_9	1.509	-0.011	-0.013
C_9—O_{11}	1.311	-0.048	-0.009
C_9—O_{10}	1.210	0.001	-0.019
O_{11}—H	0.814	-0.158	-0.192
C_8—H_a	0.974	-0.121	-0.123
C_8—H_b	0.917	-0.183	-0.181
C_5—H	1.034	-0.052	-0.052
C_4—H	0.948	-0.138	-0.139
C_7—H	0.957	-0.129	-0.129
C_6—H	1.075	-0.011	-0.011
C_2—H	1.019	-0.062	-0.062
N_1—H	0.791	-0.216	-0.216
O_{11}—C_9—O_{10}	112.7	-9.8	-11.8
O_{11}—C_9—C_8	113.5	2.9	1.2
O_{10}—C_9—C_8	123.9	-3.1	0.6
C_9—O_{11}—H	118.7	12.9	8.3
C_8—C_3—C_2	126.4	0.9	-0.1
C_3—C_2—N_1	109.7	-0.3	-0.3
C_3—C_{3a}—C_{7a}	108.8	1.7	1.6
C_3—C_2—H	124.7	-4.7	-4.7
C_3—C_{3a}—C_4	133.3	-0.8	-0.7
N_1—C_{7a}—C_7	130.8	0.5	0.3
C_{7a}—C_7—C_6	117.2	-0.2	-0.3
C_{7a}—C_7—H	121.5	0.2	0.2
C_7—C_6—C_5	121.0	-0.2	-0.2
C_7—C_6—H	119.3	-0.1	-0.1
C_6—C_5—C_4	121.5	0.4	0.4
C_6—C_5—H	112.4	-6.8	-6.9
C_4—C_{3a}—C_{7a}	117.9	-0.9	-0.9
C_4— C_{3a}—C_3	133.3	-0.8	-0.7
C_2— N_1—C_{7a}	109.9	0.8	0.8
C_2— N_1—H	136.2	10.9	10.9
C_2—C_3—C_8—C_9	95.5	-21.1	-9.7
C_3—C_8—C_9—O_{11}	-171.3	-6.3	-4.5
C_3—C_8—C_9—O_{10}	9.2	-7.7	5.4

Table 1 (continued)

	Exp.	Δ_{A^+CT}	$\Delta_{A^+CT-A^-CT}$
$C_8—C_9—O_{11}—H$	-163.4	14.3	14.5
$C_{3a}—C_3—C_8—H_b$	157.9	-12.5	-6.4
$C_7—C_{7a}—N_1—H$	4.5	4.0	4.2
$H—N_1—C_2—H$	-6.6	-5.9	-6.5
$N_1—C_2—C_3—C_{3a}$	-0.1	-0.1	-0.1
$H—C_4—C_{3a}—C_3$	1.1	-0.8	0.6
$H—C_5—C_6—C_7$	178.1	-1.3	-1.8
$C_{3a}—C_3—C_8—C_9$	-86.3	-19.7	-11.0

It should be emphasized that the rest of the calculated bond angles showed generally good agreement with experimental data.

According to the experimental and theoretical results, the indole ring is almost planar, for example, the $N_1—C_2—C_3—C_{3a}$ torsional angle is nearly zero (0.1°).

The overall view of X-ray dimer of IAA with atom labeling is shown in Fig. 2. This figure shows that the dimer is formed by the A^+CT and A^-CT conformers, which are held together by two O—H···O hydrogen bonds, with OH moiety behaving as proton donor and the C=O moiety as proton acceptor. Taking into account the disposition of the conformers present in the crystal several initial structures of dimers were considered. They were built using the structures of the monomers found by MD search [11] and combining them, taking CCT-CCT, A^+A^+T-A^-A^-T, A^+A^-T-A^-A^+T, and G^+A^+T-G^-A^-T molecules oriented in the "tail-to-tail" way. Geometry optimization of the dimers performed at the B3LYP/6-31G** level of theory was followed by the calculations of the vibrational frequencies, confirming them as local minima (Fig. 3).

The relative energies of the identified dimers with respect to the most stable (CCT-CCT) were 0.84, 2.51 and 5.0 kJ mol^{-1} for A^+A^+T-A^-A^-T, A^+A^-T-A^-A^+T, and A^+CT-A^-CT, respectively. A natural bond orbital (NBO) analysis allowed us to explain the stability order of the IAA monomers [11]. The stability order of dimers can be rationalized on the basis of the same structural factors and of the similar associated charge delocalization phenomena described through specific hyperconjugative charge transfers [11].

The relative population at 297 and 100 K calculated with Boltzman distribution shows that the CCT-CCT dimer has a relative conformational population of 45.6% at room temperature, while for the less stable dimers relative populations of 31.2%, 17.3%, and 5.9%, were found. It has to be remarked that at 100 K the relative population of the CCT-CCT dimer increases with a decrease in the population of the A^+A^+T-A^-A^-T, A^+A^-T-A^-A^+T, and A^+CT-A^-CT forms.

A comparison between the bond lengths and bond angles of A^+CT-A^-CT dimer with respect X-ray data are also shown in Table 1. For A^+CT, dihedral angles $C_2—C_3—C_8—C_9$, $C_{3a}—C_3—C_8—H_b$, $C_{3a}—C_3—C_8—C_9$ and $C_3—C_8—C_9—O_{10}$ differed from those in the CSD-INACET03 crystal in -21.1°, -12.5°, -19.7° and -7.7°, respectively and for A^+CT-A^-CT dimer that dihedral angles differed in -9.7, -6.4, -11.0 and 5.4 respectively. The differences are lower in dimer than in monomer which is related to dimerization phenomena, resonance and intermolecular interactions mentioned above.

Other relevant parameters for dimers are displayed in Table 2; between parentheses those geometric parameters which vary in monomer with respect to dimer are indicated. The geometrical features suggest the following possible intermolecular and intramolecular hydrogen-bonding interactions: $O_{10}···H_{11'}$ (and the symmetrical one $O_{10'}···H_{11}$) and $O_{10}···H_2$ in CCT-CCT dimer, $O_{10}···H_4$ in A^+A^+T-A^-A^-T dimer, $O_{11}···H_4$ in A^+A^-T-A^-A^+T dimer, and their symmetrical ones ($O_{10'}···H_{2'}$, $O_{10'}···H_{4'}$ and $O_{11'}···H_{4'}$ respectively). In our previous work similar intramolecular hydrogen bonding interactions were characterized in the corresponding IAA monomers through the theory of atoms in molecules (AIM) [11].

Vibrational spectra

In this section, we analyze the experimental infrared and Raman spectra at 297 K (Fig. 4). Since the calculated frequencies are higher than the experimental ones, mostly

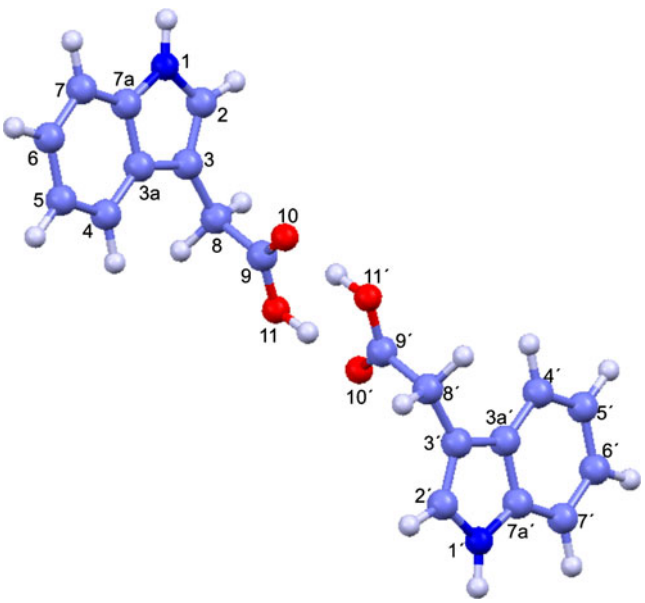

Fig. 2 Cyclic bond dimer from crystal structure optimized at B3LYP/6-31G** level

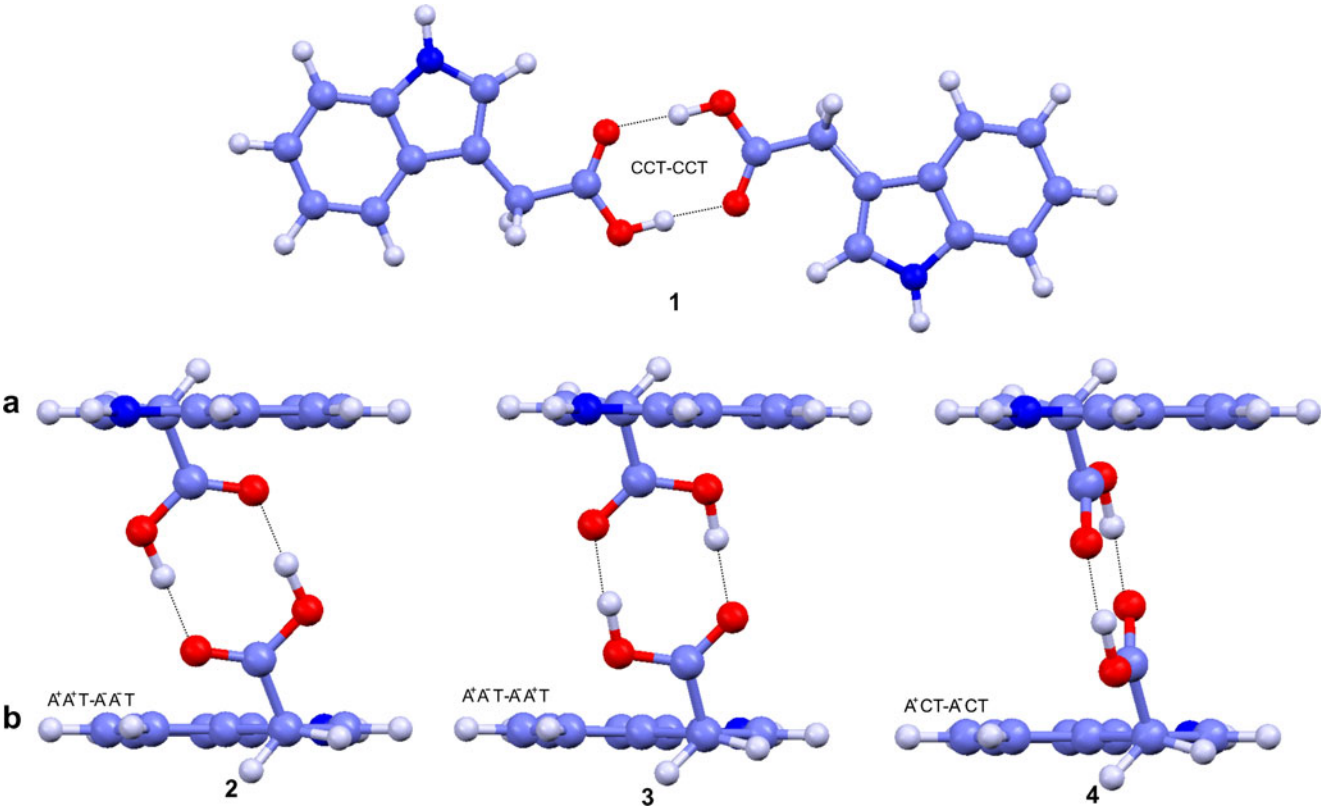

Fig. 3 Four most stable conformers of IAA dimer. The strucutres are defined by the orientation of the acetyl moieties with respect to the plane of indole ring. Dimers 2-4 are formed by two symmetrical IAA monomers one of them having the acetyl downward oriented (*Si*-face monomers, (**a**)) and the other isomer having the acetyl upward oriented (*Re*–face monomers, (**b**)). Monomers are labeled according to IUPAC recommendations: the first letter characterizes the orientation of the C_9 atom relative to the central C_3—C_8 bond, the second letter describes the C_3—C_8—C_9—O_{10} angle, and the third letter specifies the orientation of the H relative to the central C_9—O_{11}

due to limitations in the basis set, the approximated treatment of the electron correlation, and anharmonicity effects, we scaled the calculated values to reproduce the observed frequencies using a proper scaling factor taken from the Computational Chemistry Comparison and Benchmark Database (CCCBDB) [18]. The measured and calculated wavenumbers of active modes in infrared (at 100 and 297 K) and Raman (at 297 K) spectroscopy for IAA dimer are shown and described in Table 3 and in Supplementary material a detailed analysis is done.

The infrared spectra of IAA (Fig. S1, Supplementary Material) showed softening (Δ=-) and hardening (Δ=+) of several vibrational modes, thus implying subtle structural changes in the molecule as it cools down. In Supplementary material in depth description is displayed.

The assignments show two characteristics that are typically evidence for the presence of IAA dimers:

i) When the dimeric molecule is considered as a whole, two carbonyl stretching wavenumbers (symmetric and asymmetric) are expected. The dimeric molecule has a center of symmetry, so the symmetric carbonyl stretching should be Raman active only, and the asymmetric stretching should be infrared active only [19]. In the infrared spectrum wavenumbers from 1720 to 1680 cm^{-1} correspond to the asymmetric C=O stretching [19–22], in IAA this band showed a splitting with peaks at 1689 and 1702 cm^{-1}. In Raman spectrum the band corresponding to the symmetric C=O stretching should appears at 1680-1640 cm^{-1} [19, 23], in IAA, a corresponding peak was found at 1641 cm^{-1}. When the carbonyl is hydrogen bonded, but not dimerized, a band should appear at 1730-1705 cm^{-1} in both infrared and Raman spectra [19, 21].
ii) The IR wavenumber of the νC=O mode is slightly lower than the wavenumber of the non-associated carboxylic C=O group 1800-1740 cm^{-1} [19–21]. The IAA values of the corresponding vibrational mode (1689 and 1702 cm^{-1}, above mentioned) also indicates that in IAA the C=O group is involved in an intermolecular hydrogen bonding as was suggested by geometrical analysis (Table 3).

Table 2 Others relevant geometrical parameters obtained of the lowest energy IAA dimers calculated at the B3LYP/6-31G** level

	Dimers				
	CCT-CCT	A^+A^+T-A^-A^-T	A^+A^-T-A^-A^+T	A^+CT-A^-CT	Experimental
Distances (Å)					
$O_{10}\cdots H_{11'}$[a]	1.651	1.629	1.621	1.633	1.871
$O_{10}\cdots H_2$[b]	2.368 (2.363)				3.783
$O_{10}\cdots H_4$		2.765 (2.734)		3.700 (2.939)	3.859
$O_{11}\cdots H_4$			2.748 (2.752)		4.230
C_9—O_{10} (C=O)	1.232 (1.212)[c]	1.234 (1.212)	1.232 (1.210)	1.230 (1.209)	1.210
C_9—O_{11} (C—O)	1.321 (1.357)	1.316 (1.355)	1.318 (1.357)	1.320 (1.359)	1.311
O_{11}—H	1.004 (0.972)	1.008 (0.972)	1.009 (0.972)	1.007 (0.972)	0.814
C_4—H	1.087	1.085	1.085	1.087 (1.085)	0.948
C_2—H	1.078	1.081	1.081	1.081	1.019
Angles (°)					
O_{11}—H$\cdots O_{10'}$[d]	178.8	179.2	179.2	180.0	160.3
$O_{10}\cdots$H—C_2	108.3 (109.4)				
$O_{10}\cdots$H—C_4		122.2 (124.5)		92.6 (104.0)	29.5
$O_{11}\cdots$H—C_4			119.7 (117.5)		
C_9—O_{11}—H	110.3 (106.0)	110.5 (105.9)	110.6 (106.1)	110.4 (105.9)	118.7
O_{11}—C_9—O_{10}	123.6 (121.9)	124.4 (122.5)	124.4 (122.5)	124.4 (122.4)	122.7
H_a—C_8—H_b	104.2 (104.2)	108.7 (108.6)	108.7 (108.5)	105.3 (105.3)	113.7

[a] $O_{10'}\cdots H_{11}$ distance is equivalent by symmetry

[b] Distances greater than 3.700 Å are not mentioned

[c] Between parentheses those geometrical parameters which vary in monomer with respect to dimer are indicated

[d] $O_{11'}$—H$\cdots O_{10}$ angle is equivalent by symmetry

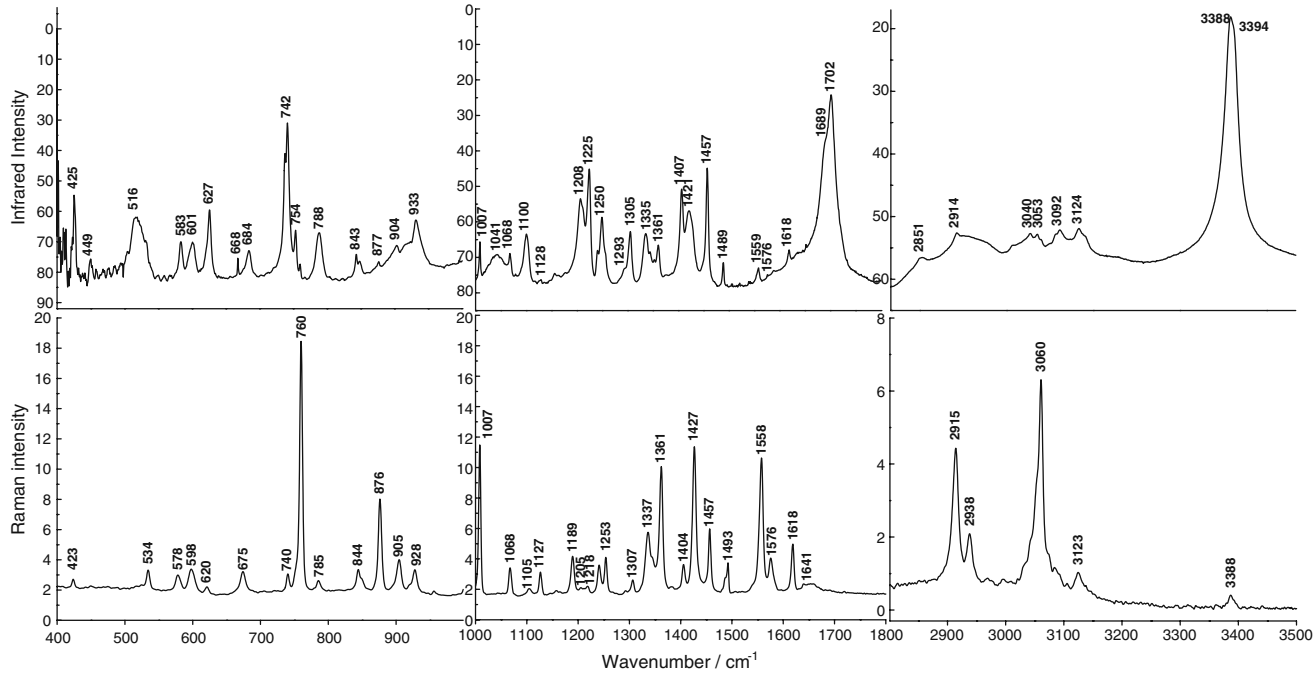

Fig. 4 Experimental infrared and Raman spectra at 297 K of *1H*-indole-3-acetic acid

Table 3 Calculated, observed and assigned wavenumbers[a] of active modes in infrared (297 and 100 K) and Raman (297 K) for IAA dimer

Theoretical wavenumbers[b]		Experimental wavenumbers[c]			Assignments[c]
Infrared	Raman	Infrared		Raman	
		297K	100K	297K	
422	421	425s	426s	423w	$\delta C_8C_9O_{11sciss}+\tau 6R$
434	434	449w	451w	449w	$\tau 6R$
525	527	516s	523, 532s	534m	$\gamma C_9O_{10}O_{11wag}+\delta 6R$
570	567	583m	584, 586m	578m	$\delta 6R$
590	586	601m	601m	598m	$\delta 6R+\delta 5R$
608	606	627s	630s	620w	$\tau 6R+\tau 5R$
677	662	684m	686m	675m	$\delta C_9O_{10}O_{11sciss}$
731	731	738, 742vs	739, 742vs	740m	$\gamma C_4H(+)+\gamma C_5H(+)+\gamma C_7H(+)+\gamma C_6H(+)$
744	743	754m	754m	760vs	$\tau 6R+\tau 5R$
797	795	788s	787, 790s	785vs	γC_2H
832	832	843m	845m	844m	$\gamma C_4H(-)+\gamma C_5H(-)+\gamma C_7H(+)+\gamma C_6H(+)$
862	861	877w	878w	876s	$\delta 6R+\delta 5R$
885	883	904m	907m	905m	$\nu C_8C_9+\delta C_9O_{10}O_{11sciss}$
991	954	933ms	943s	928m	$\gamma O_{11}H$
1010	1010	1007m	1007m	1007vs	$\delta 6R+\delta 5R$
1052	1052	1068m	1068m	1068m	$\delta 6R+\delta 5R$
1120	1120	1100s	1101s	1105w	$\delta C_4H+\delta C_5H+\delta C_6H+\delta C_7H+\delta C_2H$
1145	1145	1128vw	1128vw	1127m	$\delta C_5H+\delta C_4H+\delta C_7H+\delta C_6H$
1173	1173			1189m	$\gamma C_8H_{(2)twist}$
1210	1209	1208s, 1211s	1210s, 1213s	1205w	$\gamma C_8H_{(2)wag}+\delta 6R+\delta 5R$
1246	1243	1225vs	1226vs	1218vw	νC_9O_{11}
1296	1295	1250s	1255s	1253m	$\nu C_8C_9+\delta O_{11}H$
1339	1338	1305s	1310s	1307w	$\nu N_1C_{7a}+\nu N_1C_2+\delta 6R+\delta 5R$
1342	1342	1335s	1337s	1337s	$\delta 6R+\delta 5R$
1351	1351	1361s	1362s	1361vs	$\gamma C_8H_{(2)wag}+\nu C_{3a}C_{7a}+\nu C_5C_6+\nu C_{3a}C_3$
1360	1360	1407vs	1407vs	1404w	$\delta O_{11}H$
1418	1418	1421s	1425s	1427vs	$\delta C_8H_{(2)sciss}$
1452	1452	1457vs	1457vs	1457s	$\nu C_{3a}C_{7a}+\nu C_4C_5+\nu C_6C_7$
1491	1491	1489m	1488m	1493m	$\nu C_4C_5+\nu C_6C_7$
1564	1564	1559w	1559w	1558vs	$\nu C_2C_3+\nu C_5C_6+\nu C_7C_{7a}$
1585	1585	1576vw	1576vw	1576m	$\nu C_{3a}C_4+\nu C_5C_6+\nu C_6C_7+\nu C_{3a}C_{7a}+\nu C_2C_3+\delta N_1H$
1629	1629	1618w	1619w	1618s	$\nu C_4C_5+\nu C_{7a}C_7+\nu C_2C_3$
1737	1683	1689 vs,1702vs	1692vs, 1698vs	1641w	νC_9O_{10}
	2919			2915vs	$\nu O_{11}H$ in-phase
3035					$\nu O_{11}H$ out-of-phase
2957	2957	2851v	2847m	2938m	$\nu C_8H_{(2)sym}$
2991	2991	2914m	2913m		$\nu C_8H_{(2)asym}$
3081	3081				$\nu C_4H+\nu C_6H+\nu C_7H+\nu C_5H$
3087	3087				$\nu C_4H+\nu C_7H+\nu C_6H+\nu C_5H$
3097	3097	3040m	3128vs		$\nu C_7H+\nu C_6H+\nu C_5H+\nu C_4H$
3109	3109	3053m	3132vs	3060vs	$\nu C_5H+\nu C_4H+\nu C_7H+\nu C_6H$
3160	3160			3123w	νC_2H
3579	3579	3388vs	3378vs	3388w	νN_1H in-phase
3579	3579	3394vs	3386vs		νN_1H out-of-phase

[a] The theoretical calculated and the corresponding wavenumber assignments are in cm^{-1}

[b] Calculated infrared and Raman wavenumbers are scaled by a factor of 0.96

[c] Abbreviations: m, medium; s, strong; w, weak; v, very; ν, stretching; γ, out-of-plane bending; δ, in-plane bending; τ, torsion; sciss, scissoring; rock, rocking; wag, wagging; twist, twisting; 5R, five-membered indole ring; 6R, six-membered indole ring

Comparison of experimental Raman spectrum of IAA at 297 K and the DFT (B3LYP)/6-31G** calculated spectra for: CCT-CCT, A^+A^+T-A^-A^-T, A^+A^-T-A^-A^+T, and A^+CT-A^-CT dimers is shown in Fig. 5. As can be seen, the four predicted dimers (CCT-CCT, A^+A^+T-A^-A^-T, A^+A^-T-A^-A^+T and A^+CT-A^-CT) contribute distinctively to the assignment and interpretation of the experimental results.

When we follow the behavior of dihedral angle δ_2 interesting aspects are revealed. In fact, we can associate the CCT-CCT dimer with the A^+CT-A^-CT dimer, onward "series C" (periplanar array) according as that torsion angle is within 0° to ±30°, and A^+A^-T-A^-A^+T dimer with A^+A^+T-A^-A^-T dimer, onward "series A" (clinal array) according as that torsion angle is within ±60° to ±120° (see Fig. 6). Our results show that these structural characteristics are significant in the behavior of vibrational modes defining similar trends within each series, see Table 4. In this table the modes mainly affected by conformational changes and dimerization are shown. The bands labeling in Fig. 5 corresponds to their ordering in the Table 4 and to their ordering in the following analysis.

The band of medium intensity observed at 675 cm^{-1} in the experimental Raman spectrum correspond to in-plane angular deformation mode of $C_9O_{10}O_{11}$, observed at

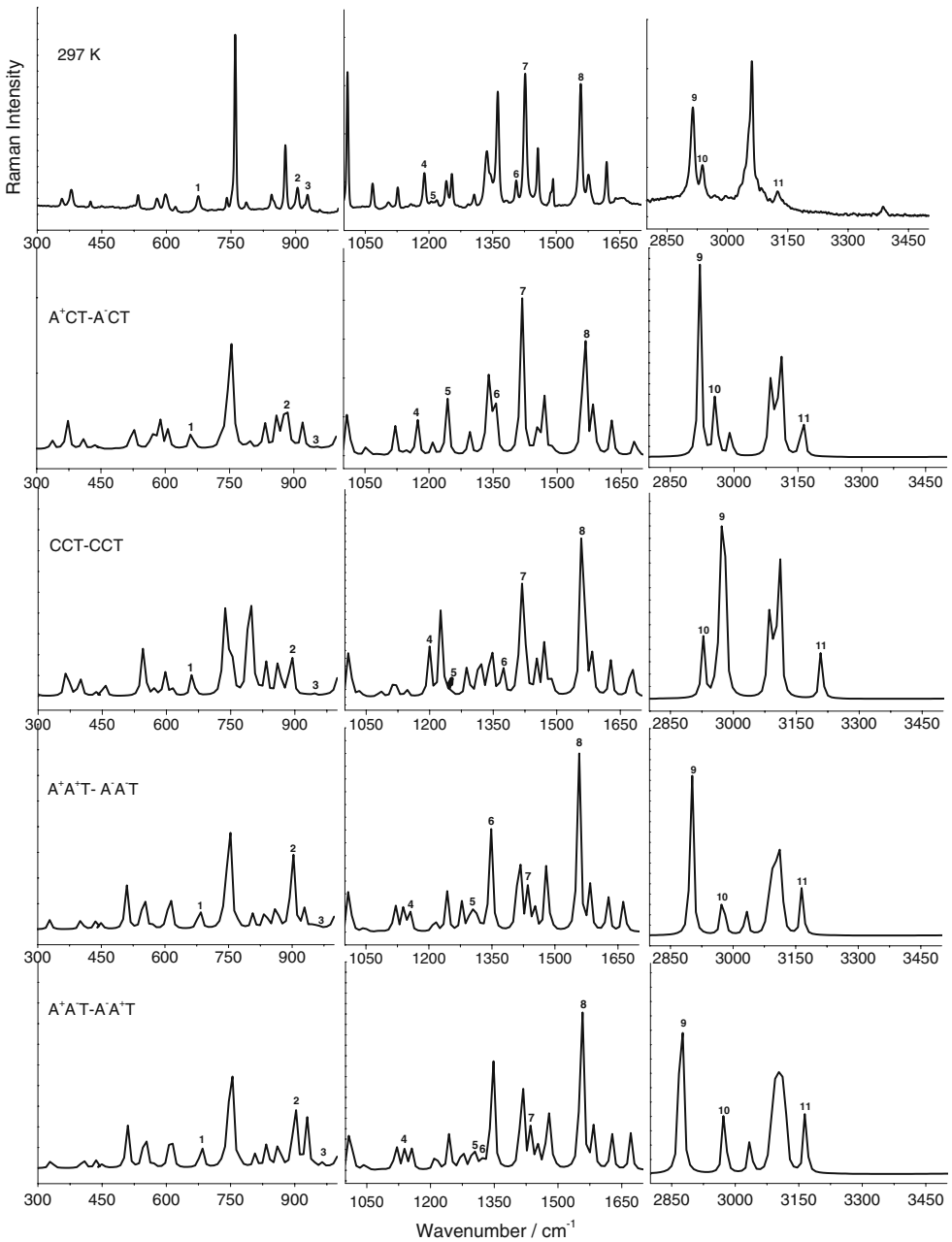

Fig. 5 Experimental Raman spectrum of IAA at 297 K and DFT (B3LYP)/6-31G** calculated spectra for: A^+CT-A^-CT, CCT-CCT, A^+A^+T-A^-A^-T and A^+A^-T-A^-A^+T. Bands labeling corresponds to their ordering in Table 4

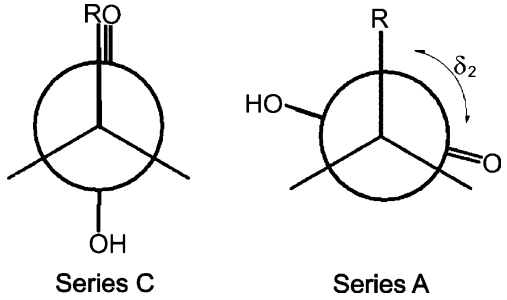

Fig. 6 Scheme of series A and C which differs in the dihedral angle δ_2

682 cm^{-1} in "series A" and at ≈ 661 cm^{-1} in "series C". Therefore the differences found in calculated frequencies of $\delta C_9O_{10}O_{11}$ mode are related to the values of dihedral angle δ_2, thus showing sensitivity with respect to the conformational changes. Our results also showed that this mode changed upon dimerization thus showing an increasement (blue shifting) of ≈ 99 cm^{-1} in the dimeric form (see Table 4, label "1"). This finding corresponds to an increase of ≈ 1.9° in $C_9O_{10}O_{11}$ angle in IAA dimer (see Table 2) as expected [23].

The band detected at 905 cm^{-1} is ascribed to the stretching mode of C_8—C_9 and in-plane angular deformation mode of $C_9O_{10}O_{11}$ (labeled as "2"). In "series A" that band appeared at 900 cm^{-1} and in "series C" that band appeared between 882 and 891 cm^{-1}. The frequencies in the dimers were blue shifted with respect to the corresponding monomers (increasement of ≈ 29 cm^{-1}). The mentioned increase of $C_9O_{10}O_{11}$ angle in IAA dimer can also be related to this behavior.

The band of medium intensity at 928 cm^{-1} was assigned to the out-of-plane angular deformation mode of O_{11}—H (labeled as "3"). In dimers this mode was highly shifted to higher frequencies (blue shifting of ≈ 316 cm^{-1}).

Other band of medium intensity at 1189 cm^{-1} arises from $C_8H_{(2)}$ twisting deformation mode (labeled as "4"). In "series A" this mode appeared at ≈ 1147 cm^{-1} and in "series C" at 1199 in CCT-CCT dimer and at 1173 cm^{-1} in A^+CT-A^-CT dimer.

The very weak band at 1218 cm^{-1} was associated to the C_9—O_{11} stretching mode (labeled as "5"). In "series A" this mode appeared at 1301 cm^{-1} and in "series C" at ≈ 1245 cm^{-1}. The C_9—O_{11} stretching mode in dimers was highly shifted to higher frequencies (blue shifting of ≈ 170 cm^{-1}). As expected a concomitant decrease of C_9—O_{11} bond length upon dimerization (see in Table 2) was found [24, 25].

The weak band at 1404 cm^{-1} is associated to O_{11}—H in-plane bending mode (labeled as "6"). This vibration in dimers was highly shifted to higher frequencies (blue shifting of ≈ 116 cm^{-1}). A concomitant increase of C_9—O_{11}—H angle was found (see Table 2) [24, 25]. Blue shifting in "series C" with respect "series A" was found.

The strong band at 1427 cm^{-1} can be attributed to the $C_8H_{(2)}$ scissoring deformation mode (labeled as "7"). This mode appeared at ≈ 1436 cm^{-1} in "series A" and at ≈ 1420 cm^{-1} in "series C". An associated decrease of ≈ 4° in

Table 4 Selected Raman wavenumbers[a] calculated at B3LYP/6-31G** level of theory for IAA dimers and monomers

Label[b]	Assignments[c]	Theoretical Raman wavenumbers[d]			
		CCT-CCT ($\Delta\nu_{monomer-dimer}$)	A^+A^+T-A^-A^-T ($\Delta\nu_{monomer-dimer}$)	A^+A^-T-A^-A^+T ($\Delta\nu_{monomer-dimer}$)	A^+CT-A^-CT ($\Delta\nu_{monomer-dimer}$)
1	$\delta C_9O_{10}O_{11sciss}$	661 (-85)	682 (-110)	682 (-110)	662 (-91)
2	$\nu C_8C_9+\delta C_9O_{10}O_{11sciss}$	891 (-27)	900 (-31)	900 (-32)	882 (-26)
3	$\gamma O_{11}H$	924 (-280)	959 (-338)	965 (-345)	954 (-301)
4	$\gamma C_8H_{(2)twist}$	1199 (-4)	1154 (-)	1140 (-)	1173 (8)
5	νC_9O_{11}	1247 (-142)	1301 (-200)	1301 (-207)	1243 (-132)
6	$\delta O_{11}H$	1379 (-106)	1355 (-152)	1326 (-117)	1360 (-90)
7	$\delta C_8H_{(2)sciss}$	1423 (1)	1436 (1)	1437 (1)	1418 (1)
8	$\nu C_2C_3+\nu C_{7a}C_7+\nu C_5C_6$	1561 (0)	1557 (0)	1556 (-2)	1564 (-2)
9	$\nu O_{11}H$	2976 (689)	2900 (759)	2872 (788)	2919 (742)
10	$\nu C_8H_{(2)sym}$	2926 (8)	2976 (-3)	2974 (-2)	2957 (-27)
11	νC_2H	3209 (-2)	3165 (-1)	3166 (-1)	3160 (0)

[a] The theoretical wavenumbers are in cm^{-1}

[b] Labeling according to Fig. 5

[c] Abbreviations: ν, stretching; γ, out-of-plane bending; δ, in-plane bending; sciss, scissoring; twist, twisting

[d] Calculated Raman wavenumbers are scaled by a factor of 0.96

H_a—C_8—H_b angle in "series C" with respect to "series A" was reported (Table 2).

The very strong band at 1558 cm^{-1} is assigned to C—C rings stretching modes (labeled as "8"). These modes appeared at ≈ 1556 cm^{-1} in "series A" and at ≈ 1562 cm^{-1} in "series C". Thus, this region is only slightly sensitive to the conformational changes. In monomers similar trends were found.

Intense band at 2915 cm^{-1} is described as due to stretching mode of O_{11}—H (labeled as "9"). Blue shifting in "series C" with respect to "series A" was found. Moreover this mode allowed us to differentiate between A^+A^-T-A^-A^+T and A^+A^+T-A^-A^-T dimers. The νO—H mode in A^+A^-T-A^-A^+T dimer appeared at 2872 cm^{-1} and the corresponding to A^+A^+T-A^-A^-T dimer appeared at 2900 cm^{-1}. The lower frequency is related to the higher bond length (see Table 2) and explained through the intramolecular $O_{11}\cdots H—C_4$ and the intermolecular $O_{10'}\cdots H—O_{11}$ H-bonds presents in A^+A^-T-A^-A^+T dimer. The O_{11}—H moiety plays as the proton acceptor in the former H-bond and as the proton donor in the latter H-bond. Therefore the dual role of the O_{11}—H moiety is related to the highest red shifting of the O_{11}—H stretching frequency. This mode is shifted to lower frequencies when the dimer is constituted (red shifting of 730 cm^{-1} on average).

Therefore our results show that the dimerization phenomena leads to increased O_{10}—C_9—O_{11} and C_9—O_{11}—H bond angles; which can be related to a blue shifting of associated bending modes ($\delta C_9O_{10}O_{11}$ and $\delta C_9O_{11}H$). Moreover a decrease (increase) in C_9—O_{11} (O_{11}—H) bond distance was found; which can be related with a blue (red) shifting of associated stretching mode.

Symmetric stretching vibration of $C_8H_{(2)}$ were recorded and assigned as the band of medium intensity located at 2938 cm^{-1}. Lower frequencies at "series C" were found.

In our previous work we performed a thorough NBO analysis of monomeric forms which allowed us to explain the features that characterize and differentiate the "series A" with respect to "series C" [11]. It is worth noting that the same description can be used to analyze the observed blue or red shifting of the vibrational frequencies belonging to "series C" with respect to "series A", allowing us to get deeper insights in the light of charge delocalization effects. For example, the red shifting of νC_9O_{11} in "series C" can be related with higher charge transfer from C_3—O_8 bonding orbital to the C_9—O_{11} antibonding orbital, similarly the red shifting of $\nu O_{11}H$ in "series A" can be related with higher charge transfer from C_8—C_9 bonding orbital to the O_{11}—H antibonding orbital [11].

The other band of medium intensity at 3123 cm^{-1} arises from the stretching mode of C_2—H. This mode appeared at ≈ 3164 cm^{-1} in A^+A^+T-A^-A^-T, A^+A^-T-A^-A^+T, and A^+CT-A^-CT dimers; besides in CCT-CCT dimer this mode is blue shifted in ≈ 45 cm^{-1}. These findings allowed us to differentiate between conformer CCT-CCT from all the others.

The better reproduction of measured values are achieved by A^+CT-A^-CT dimer, as can be seen in Fig. 5, thus according to the CSD-INACET03 X-ray structure. Within 300 and 1000 cm^{-1}, the Raman bands corresponding to in-plane deformation mode of $C_8C_9O_{11}$, rocking mode of $C_8H_{(2)}$, in-plane deformation mode of $C_9O_{10}O_{11}$ were very similar to the measured ones. Within 2800 y 3600 cm^{-1} the higher difference between calculated and measured wavenumbers were found for CCT-CCT, A^+A^+T-A^-A^-T and A^+A^-T-A^-A^+T dimers.

By deconvolution of the corresponding band to νC=O in the infrared spectrum, we observed the existence of two peaks (Fig. 7a). According to our theoretical results the A^+A^+T-A^-A^-T, CCT-CCT and A^+A^-T-A^-A^+T dimers con-

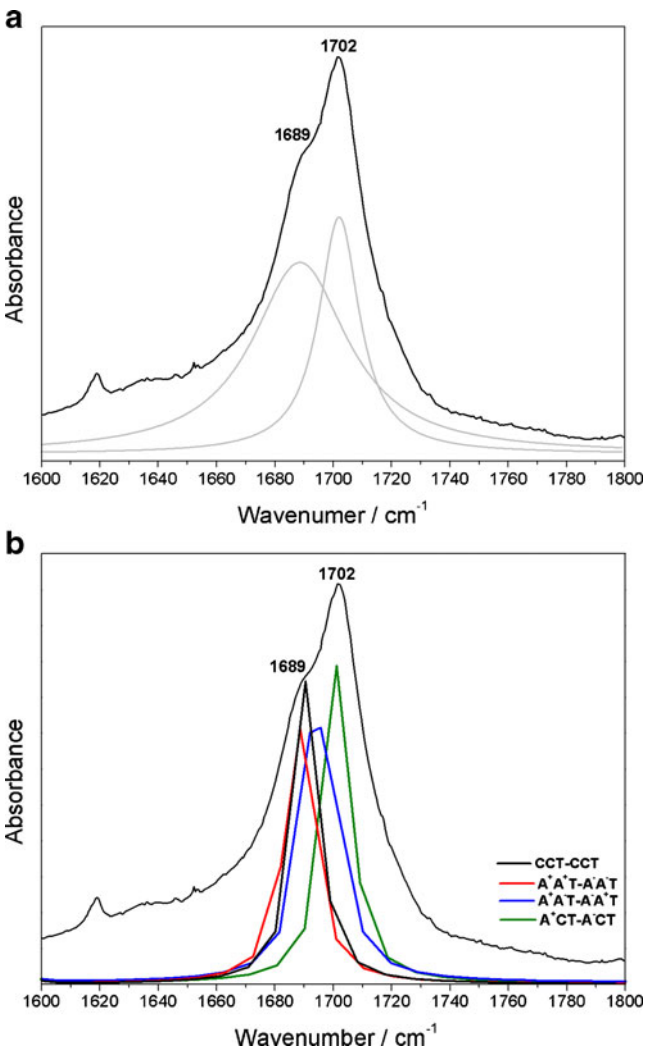

Fig. 7 Band deconvolution for the C=O stretching mode in IAA at 297 K (**a**) and the theoretical contributions of IAA dimers (**b**)

tribute to the first band, and the A^+CT-A^-CT dimer to the second and more intense band (Fig. 7b). The results suggest that our sample is made of large domains in which only one of the conformers is present. This spectral region is considered as characteristic and fundamental for use in the study of the conformational equilibrium, thus indicating a conformational equilibrium involving those non-equivalent IAA dimers [23, 26] and thus according with a polycrystalline sample.

Conclusions

Theoretical studies on dimers of *1H*-indole-3-acetic acid were performed to investigate the conformational properties and vibrational spectra. Experimental infrared spectra at 100 K and 297 K and Raman spectrum at 297 K was analyzed and compared against *ab-initio* calculations performed at B3LYP level. The assignment of the vibrational modes of the IAA, calculated at the B3LYP/6-31G** level, was shown, and discussed as well.

The conformational space of IAA monomeric molecule and X-ray data were utilized to obtain the geometry of the lowest-energy IAA dimers. Four dimeric conformers were obtained and classified. In stability order they are: CCT-CCT, A^+A^+T-A^-A^-T, A^+A^-T-A^-A^+T, and A^+CT-A^-CT dimers. The analysis of the experimental infrared and Raman data performed by comparison against theoretical calculation showed a conformational equilibrium at 297 K involving the theoretically predicted dimeric forms that contribute distinctively to the assignments of the experimental results.

We were able to identify the modes mainly affected by conformational changes and dimerization. We showed that dimerization increase O_{10}—C_9—O_{11} and C_9—O_{11}—H bond angles and that consequently blue shifted vibrational frequencies of related bending modes were found. Also we showed the decrease (increase) of C_9—O_{11} (O_{11}—H) bond length upon dimerization and the consequent blue (red) shifting of related stretching vibrational frequencies. We detect modes that allowed us to distinguish between conformers belonging to "series A" (clinal array) from the others belonging to "series C" (periplanar array), in other words we characterize modes which are more sensitive to conformational and geometrical aspects like the values of C_3—C_8—C_9—O_{10} dihedral angle. Moreover, we found that the mode νOH allows to differentiate between the conformers within "series A" (A^+A^-T-A^-A^+T and A^+A^+T-A^-A^-T dimers), and the mode νC_2H allows to distinguish the conformer CCT-CCT from all the other dimers. We also show that the dual role of the OH moiety in IAA dimers leads to the highest red-shifting in the stretching frequency of OH moiety. Work along a deep characterization of hydrogen bonding interactions present in dimeric systems is in progress in our laboratories.

Acknowledgments Thanks are due to Agencia de Promoción Científica y Tecnológica Argentina (MINCYT), CONICET and Universidad Nacional de La Plata (Argentina) for financial support. A.H.J. is Member of the Scientific Research Career (CIC, Provincia de Buenos Aires). A.A.V. is a Research Member of the National Research Council of Argentina (CONICET). M.C.P.S. acknowledges a fellowship (IP-PRH N^0 54) from Agencia de Promoción Científica y Tecnológica Argentina and Universidad de la Cuenca del Plata (Corrientes, Argentina) and R.M.L. acknowledges Universidad de la Cuenca del Plata for facilities provided during the course of this work.

References

1. Kiralj R, Ferreira MMC (2005) Chemometric and molecular modeling study of 1*H*-Indole-3-acetic acid derivates with auxin activity. Croat Chem Acta 78:541–549
2. Woo EJ, Marshall J, Bauly J, Chen JG, Venis M, Napier RM, Pickersgill RW (2002) Crystal structure of auxin-binding protein 1 in complex with auxin. EMBO J 21:2877–2885
3. Kiralj R, Ferreira MMC (2003) Combined computational and chemometric study of 1*H*-Indole-3-acetic acid. Int J Quantum Chem 95:237–251
4. Degen A, Bolte M (2001) The twinned crystal structure of 3-indoleylacetic acid. Acta Crystallogr 57:999–1000
5. Karle IL, Britts K, Gum P (1964) Crystal and molecular structure of 3-indolylacetic acid. Acta Crystallogr 17:496–499
6. Chandrasekhar K, Raghunathan S (1982) A reinvestigation of the structure of (3-indolyl)acetic acid. Acta Crystallogr B38:2534–2535
7. Pfeiffer D, Kutschabsky L, Leibnitz P, Adam G (1987) Refinement of the structure of 3-indolylacetic acid. Cryst Res Technol 22:K1–K4
8. Nigovic B, Antolic S, Kojic-Prodic B, Kiralj R, Magnus V, Salopek-Sondi B (2000) Correlation structural and physicochemical parameters with the bioactivity of alkylated derivated of indole-3-acetic acid, a phytohormone (auxin). Acta Crystallogr B 56:94–111
9. Morzyk-Ociepa B, Michalska D, Pietraszko A (2004) Structures and vibrational spectra of indole carboxylic acids. Part I. Indole-2-carboxylic acid. J Mol Struct 688:79–86
10. Morzyk-Ociepa B, Michalska D, Pietraszko A (2004) Structures and vibrational spectra of indole carboxylic acids. Part II. 5-Methoxyindole-2-carboxylic acid. J Mol Struct 688:87–94
11. Pérez Schmit MC, Jubert AH, Vitale A, Lobayan RM (2010) Electronic structure and conformational properties of 1*H*-Indole-3-Acetic Acid. J Mol Model, doi:10.1007/s00894-010-0804-7
12. HyperChem Release 7.5, Hypercube Inc., USA
13. Frisch MJ, Trucks GW, Schlegel HB, Scuseria GE, Robb MA, Cheeseman JR, Montgomery JA, Vreven T, Kudin KN, Burant JC, Millam JM, Iyengar SS, Tomasi J, Barone V, Mennucci B, Cossi M, Scalmani G, Rega N, Petersson GA, Nakatsuji H, Hada M, Ehara M, Toyota K, Fukuda R, Hasegawa J, Ishida M, Nakajima T, Honda Y, Kitao O, Nakai H, Klene M, Li X, Knox JE, Hratchian HP, Cross JB, Adamo C, Jaramillo J, Gomperts R, Stratmann RE, Yazyev O, Austin AJ, Cammi R, Pomelli C, Ochterski JW, Ayala PY, Morokuma K, Voth GA, Salvador P, Dannenberg JJ, Zakrzewski VG, Dapprich S, Daniels AD, Strain MC, Farkas O, Malick DK, Rabuck AD, Raghavachari K, Foresman JB, Ortiz JV, Cui Q, Baboul AG, Clifford S, Cioslowski J, Stefanov BB, Liu G, Liashenko A, Piskorz P, Komaromi I, Martin RL, Fox DJ, Keith T, Al-Laham MA, Peng CY,

Nanayakkara A, Challacombe M, Gill PMW, Johnson B, Chen W, Wong MW, Gonzalez C, Pople JA (2003) Gaussian 03, Revision B.02. Gaussian Inc, Pittsburgh
14. Becke AD (1993) Density-functional thermochemistry III. The role of exact exchange. J Chem Phys 98:5648–5652
15. Lee C, Yang W, Parr RG (1988) Development of the Colle-Salvetti correlation energy formula into a functional of the electron density. Phys Rev B 37:785–789
16. Chemistry IUPAC (1976) Rules for the nomenclature of organic chemistry, section E. Stereochemistry. Pure Appl Chem 45:11
17. Glusker JP, Lewis M, Rossi M (1994) Crystal structure analysis for chemists and biologists. Wiley, New York
18. National Institute of Standards and Technology; Computational Chemistry Comparison and Benchmark Database, Release 15a; Standard Reference Database Number 101, April 2010; http://srdata.nist.gov/cccbdb/
19. Colthup NB, Daly LH, Wiberley SE (1964) Introduction to infrared and Raman spectroscopy. Academic Press, New York-London
20. Nyquist RA (2001) Interpreting infrared, Raman, and nuclear magnetic resonance spectra. Academic Press, USA
21. Socrates G (2001) Infrared and Raman characteristic group frequencies: tables and charts, 3rd edn. Wiley, Oxford, England
22. Smith BC (1999) Infrared spectral interpretation: a systematic approach. CRC Press, USA
23. Mayo DW, Miller FA, Hannah RW (2003) Course notes on the interpretation of infrared and Raman spectra. Wiley, New York USA
24. Florio GM, Zwier TS, Myshakin EM, Jordan KD (2003) Theoretical modeling of the OH stretch infrared spectrum of carboxylic acid dimers based on first-principles anharmonic couplings. J Chem Phys 118:1735–1746
25. Emmeluth C, Suhm MA, Luckhaus D (2003) A monomers-in-dimers model for carboxylic acid dimers. J Chem Phys 118:2242–2255
26. Rao CNR (1963) Chemical Applications of infrared Spectroscopy. Academic, New York